Observing the orbital angular momentum of Fe and Co in chiral magnet $Fe_{0.75}Co_{0.25}Si$ using soft x-ray magnetic circular dichroism

M. Mito[1,2],* M. Ohkuma[1], T. Tajiri[3], Y. Kousaka[2,4], J. Akimitsu[5], K. Inoue[2,6,7], and K. Amamiya[8]
[1] *Graduate School of Engineering, Kyushu Institute of Technology, Kitakyushu 804-8550, Japan*
[2] *Center for Chiral Science, Hiroshima University, Higashihiroshima 739-8526, Japan*
[3] *Faculty of Science, Fukuoka University, Fukuoka 814-0180, Japan*
[4] *Graduate School of Engineering, Osaka Prefecture University, Sakai 599-8570, Japan*
[5] *Research Institute for Interdisciplinary Science, Okayama University, Okayama 700-8530, Japan*
[6] *Graduate School of Science, Hiroshima University, Higashihiroshima 739-8526, Japan*
[7] *Institute for Advanced Materials Research, Hiroshima University, Higashihiroshima 739-8526, Japan and*
[8] *Institute of Materials Structure Science, High Energy Accelerator Research Organization (KEK), Tsukuba 3050801, Japan*
(Dated: March 18, 2022)

The intermetallic compound $Fe_{1-x}Co_xSi$ has a helical magnetic order for $0.05 < x < 0.8$, whereas its orbital angular momentum contributing to the occurrence of a Dzyaloshinskii–Moriya interaction has not yet been verified. We applied soft x-ray magnetic circular dichroism spectroscopy on the Fe $L_{2,3}$ and Co $L_{2,3}$ edges below T_c for $Fe_{0.75}Co_{0.25}Si$, such that their orbital magnetic moments m_{orb} were evaluated independently. The dichroic signals provide direct experimental evidence that m_{orb} for both Fe and Co are coupled in a parallel manner with their spin counterparts m_{spin}. The ratio of m_{orb} to m_{spin} is independently estimated as $m_{orb}/m_{spin} \sim 3\%$ for Fe and 9% for Co. By comparing the average of the two m_{spin} values with the saturated magnetization using a commercial superconducting quantum interference device (SQUID) magnetometer, the hole number in the d bands for both Fe and Co is roughly estimated as approximately 1.5. This suggests that Fe and Co should be arranged closely for stabilizing the ferromagnetic moments.

I. INTRODUCTION

The Dzyaloshinskii–Moriya (DM) interaction [1, 2] is driven by the spin-orbit coupling (SOC) and crystalline chirality. In general, SOC is weaker compared to other interactions (*e.g.*, the crystalline field, orbital hybridization, and exchange interaction). The DM interaction arises from a combined second-order perturbation of SOC followed by an exchange interaction, such that the DM is linear in the SOC. The DM interaction stabilizes a magnetic ground state with a spiral order of long-wavelength. However, even within representative helical magnets, a quantitative understanding regarding the origin of the DM interaction, *i.e.*, the orbital angular momentum L, has not been sufficiently obtained.

As only an exception, in a typical monoaxial chiral magnet, $CrNb_3S_6$ (space group $P6_322$), an experimental evaluation of L and a theoretical description of the origin have been documented [3]. The expected value of the orbital magnetic moment m_{orb} for $CrNb_3S_6$ was evaluated as $|m_{orb}| = 2.3 \times 10^{-2}\ \mu_B$. The ratio of m_{orb} to the expected value of the spin magnetic moment m_{spin} is approximately 1%.

As the second non-centrosymmetric target, we focus on a so-called B20 type material, $Fe_{1-x}Co_xSi$, which has two magnetic ions [4]. Both parent compounds FeSi and CoSi, as well as their mixtures, $Fe_{1-x}Co_xSi$, commonly have a B20 type crystal structure (space group $P2_13$), where all transition-metal sites are crystallographically equivalent. Both parent compounds FeSi and CoSi are nonmagnetic. The insertion of Co into the Fe sites triggers the helimagnetic phase. For $0.05 < x < 0.8$, however, it is helical magnetic ordered, and the critical temperature T_c is maximum at $x = 0.35$ [5–11], as shown in Fig. 1(a) [6–9, 11]. In $Fe_{1-x}Co_xSi$, the valences of Fe and Co in an intermetallic compound have yet to be determined. Both elements have m_{orb} and m_{spin}, and participate in the formation of the helimagnetic order. Furthermore, a skyrmion lattice appears in the vicinity of T_c [4, 11]. Thus, in terms of the development of ferromagnetic moments and DM interactions in a distorted alloy, $Fe_{1-x}Co_xSi$ is an interesting compound.

Based on studies on the simple substances Fe and Co, Fe has a slightly larger m_{orb}/m_{spin} than Co [12]; m_{orb}/m_{spin} value is 4.3% for Fe and 3.4% for Co. In a Heusler compound, m_{orb}/m_{spin} for Co is 6.9% [12]. It is important to determine the essential role of Co in the formation of the helimagnetic phase in $Fe_{1-x}Co_xSi$. Thus, we focus on $Fe_{0.75}Co_{0.25}Si$ with the maximum values of helix wave vectors k and DM energy, as shown in Fig. 1(b) [6–9, 11], and in its composition, we conducted soft x-ray magnetic circular dichroism (MCD) spectroscopy on the Fe $L_{2,3}$ and Co $L_{2,3}$ edges ($2p \rightarrow 3d$ photoabsorption) below T_c, to directly measure m_{orb}/m_{spin} for both Fe and Co elements. These information is useful to understand the atomic configuration for the appearance of the ferromagnetic moments in a distorted alloy and the angular momentum of each atom, giving rise to a DM interaction.

The XMCD spectroscopy is a powerful tool to obtain the magnetic information for selected elements, and furthermore the analysis of the XMCD spectrum yields the

*Electronic address: mitoh@mns.kyutech.ac.jp

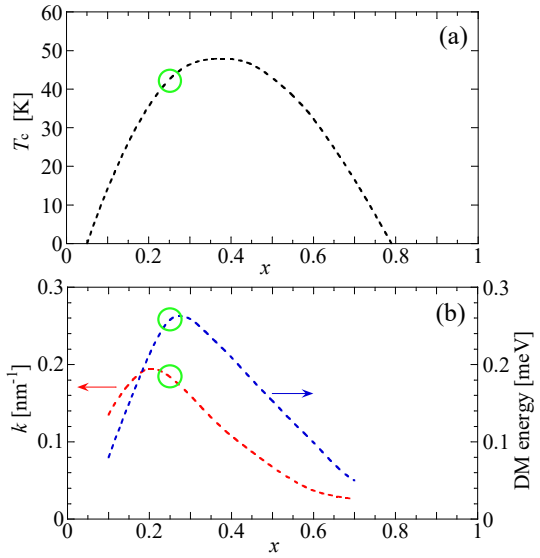

FIG. 1: (Color online) (a) x dependence of T_c and average electrons in d-orbitals for $Fe_{1-x}Co_xSi$ [6–9, 11]. (b) x dependence of helix wave vector k and DM interaction for $Fe_{1-x}Co_xSi$ [6–9, 11]. Each value corresponding to $x = 0.25$ is marked with an open green circle.

information of m_{orb} and m_{spin} for them. According to the sum rule [13–16], the orbital and spin magnetic moments of the $3d$ shell, in μ_B, (m_{orb} and m_{spin}), and the number of holes in the same shell (n_h), obey

$$\frac{\int(\mu_- - \mu_+)d\omega}{\int(\mu_+ + \mu_- + \mu_0)d\omega} = \frac{1}{2}\frac{m_{orb}}{n_h}, \quad (1)$$

$$\frac{\int_{j_+}(\mu_- - \mu_+)d\omega - 2\int_{j_-}(\mu_- - \mu_+)d\omega}{\int(\mu_+ + \mu_- + \mu_0)d\omega} = \frac{1}{3}\frac{m_{spin}}{n_h}, \quad (2)$$

where μ_q denotes the photoabsorption spectrum with a photon spin q ($=+,-,0$). The $+$ label represents the circularly polarized photons with a positive angular momentum in the direction of the wave vector, whereas the $-$ label represents those with a negative angular momentum in the direction of the wave vector. Here, μ_0 is generally defined as the average of μ_+ and μ_-. The final states are classified into $j_+(2p_{3/2})$ and $j_-(2p_{1/2})$ excitations, and the L_3 and L_2 edges are well-separated in terms of energy. In the numerator of Eq. (2), the XMCD spectrum must be integrated separately at each edge. The angle-averaged intensity of the L_3 and L_2 combinations is directly proportional to the total number of d states above the Fermi level, that is, the number of holes within the d band (n_h). Combining both Eqs. (1) and (2) yields the following expression without n_h,

$$\frac{\int(\mu_+ - \mu_-)d\omega}{\int_{j_+}(\mu_+ - \mu_-)d\omega - 2\int_{j_-}(\mu_+ - \mu_-)d\omega} = \frac{3}{2}\frac{m_{orb}}{m_{spin}}. \quad (3)$$

In $CrNb_3S_6$, splitting the L_3 and L_2 absorptions is difficult. However, the n_h value is assumed for magnetization measurements and band calculations [3]. In the present intermetallic compound, $Fe_{1-x}Co_xSi$, the charge valences of both Fe and Co have not been determined. Thus, the analysis using Eq. (3) is trustworthy.

II. EXPERIMENTAL PROCEDURES

A single crystal of $Fe_{0.75}Co_{0.25}Si$ was grown by a laser-diode-heated floating zone method (equipped with five 200 W lasers, Crystal Systems Corporation) under an Ar atmosphere [17]. The crystal size was 2 mm × 2 mm × 4 mm, and the mass was 87.5 mg. Laue x-ray diffraction with an imaging plate revealed that the obtained sample formed a single crystalline domain. To evaluate the crystallographic chirality of the sample, we cut some small portions, and examined them by means of x-ray oscillation photograph. The data were collected by Rigaku XtaLAB mini II with Mo $K\alpha$ radiation at room temperature. The absolute structure was determined using the SHELXL software package [18]. All the portions were determined to form left-handed B20 crystal structure. Thus, crystallographic chirality of $Fe_{0.75}Co_{0.25}Si$ in this study is left-handed. Grigoriev *et al.* reported that the structural chirality changes from right-handed for $x < 0.2$ to left-handed for $x > 0.2$ [19]. The left-handed chirality in the present single crystal suggests that the x value of the crystal is larger than 0.2. Figure 2 shows the magnetic field H dependence of magnetization M at 1.8 K, which is sufficiently lower than the T_c of 44 K, observed using a commercial superconducting quantum interference device (SQUID) magnetometer. The critical field for the transition to the forced ferromagnetic state, H_c, is 0.2 Tesla, and the saturated M is $1.84 \times 10^{-1}\mu_B$ per $Fe_{0.75}Co_{0.25}$. The T_c and H_c values are quite close to those of $Fe_{0.70}Co_{0.30}Si$, whose magnetic properties have been investigated in detail [20, 21]. Thus, we recognize that the present composition ratio of Co, $x = 0.25$, determined from the preparation ratio is appropriate.

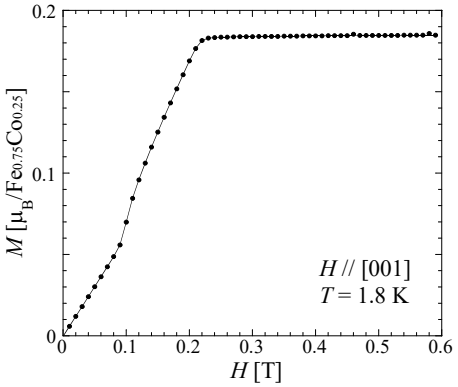

FIG. 2: (Color online) M-H curve of $Fe_{0.75}Co_{0.25}Si$ at $T = 1.8$ K, observed using a commercial SQUID magnetometer. The direction of the magnetic field was in the [001] direction.

Soft x-ray MCD (XMCD) spectroscopy was conducted on the beam line BL16A of KEK-PF. The photoabsorption spectra were obtained by directly measuring the intensity of the electron yield XMCD. The measurements were conducted at 23.9 ± 1.5 K, which is lower than T_c. Here, H was applied parallel to the [001] direction, parallel to the propagation vector of the helimagnetic modulation [4]. The x-ray beam was nearly parallel to H of 1.2 T, which was much larger than H_c. The m_{orb} and m_{spin} values for Fe and Co are evaluated using the XMCD for the forced ferromagnetic state. The obtained results should be the same as those for other crystal orientations such as [110] and [111]. When H^+ and H^- are defined as parallel and antiparallel to the light, the deviation between the left(L)-handed μ_+ and right(R)-handed μ_- is observed under four settings: L-R at H^+, L-R at H^-, R-L at H^+, and R-L at H^-. The above series of energy scans was repeated five times and the data were averaged.

The four types of integrals in Eqs. (1)-(3) are expressed as A, B, C, and D as follows:

$$\int(\mu_- - \mu_+)d\omega = A, \quad (4)$$

$$\int(\mu_- + \mu_+)d\omega = B, \quad (5)$$

$$\int_{j_+}(\mu_- - \mu_+)d\omega = C, \quad (6)$$

$$\int_{j_-}(\mu_- - \mu_+)d\omega = D, \quad (7)$$

where $A = C + D$. Thus, we can simplify Eqs. (1)-(3), as Eqs. (8)-(10),

$$A/(\frac{3}{2}B) = \frac{1}{2}\frac{m_{orb}}{n_h}, \quad (8)$$

$$(C-2D)/(\frac{3}{2}B) = \frac{1}{3}\frac{m_{spin}}{n_h}, \quad (9)$$

$$A/(C-2D) = \frac{3}{2}\frac{m_{orb}}{m_{spin}}. \quad (10)$$

In $Fe_{1-x}Co_xSi$, the valence numbers of Fe and Co have not been evaluated yet, and therefore the estimation of n_h is unreliable. Consequently, the direct evaluation of m_{orb}/m_{spin} using Eq. (10) is trustworthy.

III. XAS AND XMCD RESULTS

A. XMCD

Figure 3 shows the XAS spectra at $H = 1.2$ T. The spectra for the left (L) and right (R) polarized light beams, μ_+ and μ_-, respectively, are depicted in the figure. A set of L_3 and L_2 absorptions appeared at approximately 705-730 eV for Fe and 775-800 eV for Co, respectively, as described in the literature [22]. In the XAS of Fe at the L_3 and L_2 edges, a small XAS owing to oxidization was observed following the maximum XAS. The XMCD spectrum of (μ_- - μ_+) was also documented. The XMCD signal for Fe is larger than that for Co. The influence of oxidization on the XMCD is mentioned for each step in a series of analyses, the details of which are listed in Tables I and II.

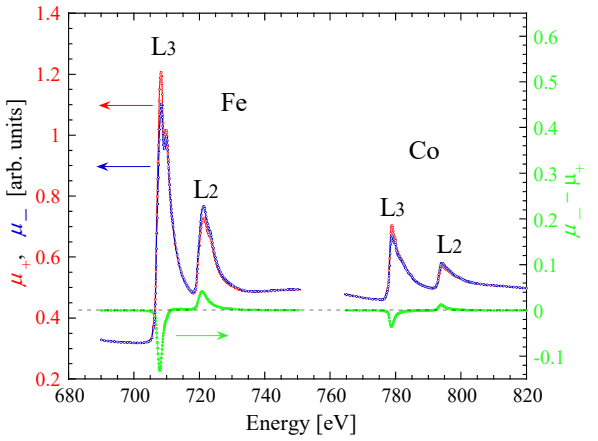

FIG. 3: (Color online) XAS profiles for the left- and right-handed circularly polarized light beams (μ_+, red) and (μ_-, blue), respectively, and XMCD spectra (μ_- - μ_+, green) for $Fe_{0.75}Co_{0.25}Si$ at $H = 1.2$ T and $T = 23.9 \pm 1.5$ K. A set of L_3 and L_2 absorptions appear at 705-730 eV for Fe and the 775-800 eV for Co, respectively.

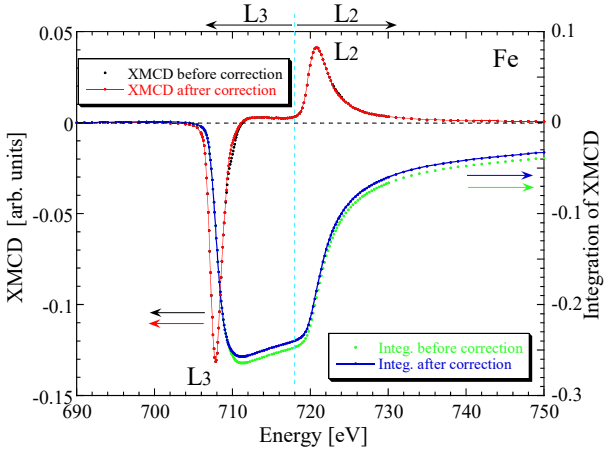

FIG. 4: (Color online) XMCD spectra, $\mu_- - \mu_+$, at $H = 1.2$ T for Fe in $Fe_{0.75}Co_{0.25}Si$. The integration of XMCD with respect to an increase in energy is shown on the right vertical axis. For reference, the analysis after subtracting the oxide component (XMCD, red; and its integration, blue) was compared to that before calibration (XMCD, black; and its integration, green).

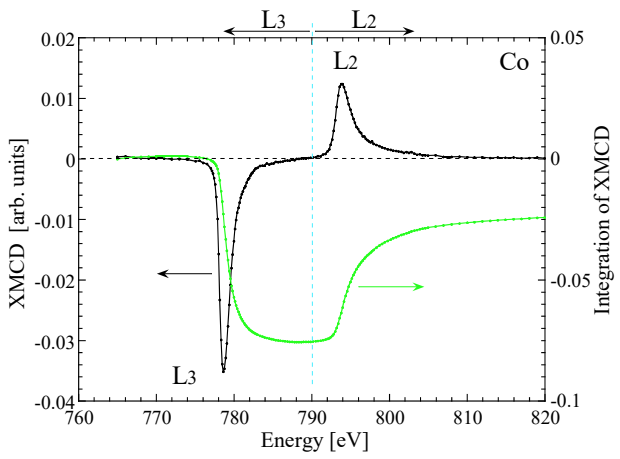

FIG. 5: (Color online) XMCD spectra, $\mu_- - \mu_+$, at $H = 1.2$ T for Co in $Fe_{0.75}Co_{0.25}Si$. The integration of XMCD with respect to an increase in energy is shown on the right vertical axis. In the present XMCD data for Co, subtraction of the oxide component is not necessary.

The XMCD profiles of Fe and Co are shown in Figs. 4 and 5, respectively, along with the XMCD integration with respect to energy. The integration value becomes finite for both Fe (see Fig. 4) and Co atoms (see Fig. 5), which suggest that L exists for both. First, we calculate the numerator on the left-hand side of Eq. (10). We focus on the integration of the resultant XMCD spectra (μ_--μ_+) with respect to energy, namely A, where A is estimate to be -3.25 $\times$ 10^{-2} for Fe and -2.42 $\times$ 10^{-2} for Co (see Table I). The signal from the oxide component at the surface prominently appears at L_3 rather than at L_2, which was observed significantly in the energy region for Fe. The contribution of oxidization is presented in Table I, and cannot be numerically neglected for Fe.

Next, we estimate the denominator on the left-hand side of Eq. (10). The XMCD ratio at L_3 between Fe and Co is approximately 3.7:1.0, which is slightly larger than their composition ratio. Regarding Fe, we propose the border of the L_3 and L_2 areas as 718 eV, above which the XMCD of L_2 begins to increase following the change in L_3, and then we estimate the integration value of XMCD for both the low- and high-energy sides. Consequently, we obtained C = -2.39 $\times$ 10^{-1} and D = 2.06 $\times$ 10^{-1} as the integrals appearing in the denominator on the left-hand side of Eq. (10). As a result, we directly obtain $m_{\rm orb}/m_{\rm spin}$ = 3.33 $\times$ 10^{-2}. This value is overestimated by 16% if the oxide contribution is not subtracted from the XMCD spectrum (see Table II).

Regarding Co, we propose the border of the L_3 and L_2 areas as 790 eV, above which the XMCD of L_2 begins to increase following the change in L_3, and we estimate the integration value of XMCD for both the low- and high-energy sides. Consequently, we obtained C = -7.54 $\times$ 10^{-2} and D = 5.12 $\times$ 10^{-2} as the values of the integrals appearing in the denominator on the left-hand side of Eq. (10). As a result, we directly obtained $m_{\rm orb}/m_{\rm spin}$ = 9.07 $\times$ 10^{-2}. In the Co spectrum, the insertion of the oxide contribution is small. The value of $m_{\rm orb}/m_{\rm spin}$ shows little change, even if the oxide contribution is not subtracted in the XMCD spectrum. Details of the analytical results obtained by subtracting the oxidization effects are presented in Tables I and II. It should be noted that oxidization occurs on the surface of the crystal, particularly for the Fe atoms. The signal from the oxidization does not originate from the nature of the bulk crystal.

B. XAS

Figure 6(a) shows the spectra of $\mu_- + \mu_+$ at $H = 1.2$ T for Fe with a green profile. It has a background constructed through a combination of two linear-like terms, labeled BKG-1. The profile after subtracting BKG-1 is depicted with red color. The resultant profile has another background composed of two arctangent functions, labeled BKG-2. The profile after subtracting BKG-2 is shown in Fig. 6(b). The ratio of the two arctangent function intensities is consistent with the XAS intensities for L_3 and L_2. The effect of oxidization appears more prominently in L_3 than in L_2. The integration of the final XAS obtained after subtracting the oxide components yields a value of B = 1.09 $\times$ 10^1. For reference, the same analytical results for the XAS without subtracting the oxide components yielded B = 1.13 $\times$ 10^1. The same procedure was also followed for Co, as depicted in Fig. 7. For Co, the influence of oxidization in XAS is quite small, as indicated in Table I, and the value of B is barely revised even when subtracting the oxide component.

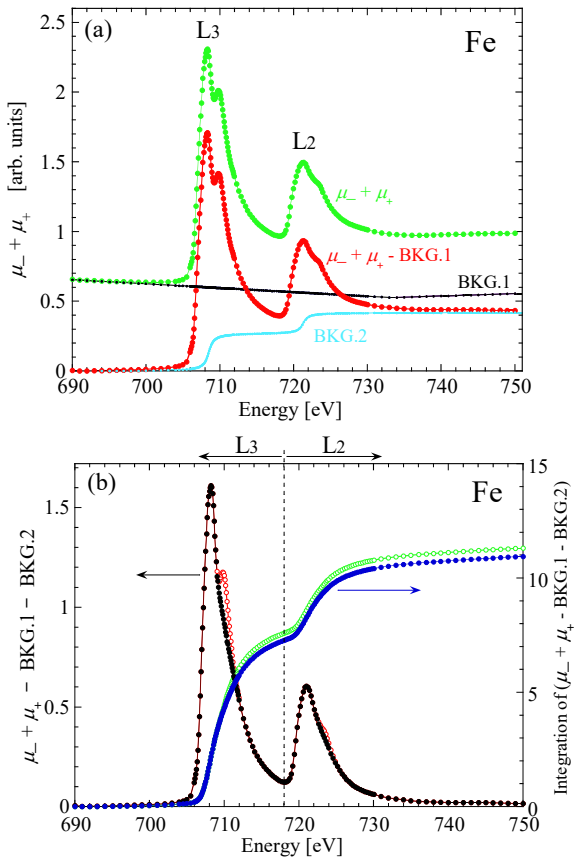

FIG. 6: (Color online) (a) XAS profile $\mu_- + \mu_+$ for Fe at H = 1.2 T. The residual XAS profile obtained after subtracting the assumed background (BKG.1) is shown along with BKG.2, which is composed of two arctangent functions (intensity ratio of 1.8:1.0). (b) XAS profiles after subtracting two background components (BKG.1 and BKG.2), $\mu_- + \mu_+$ - BKG.1 - BKG.2, for Fe at H = 1.2 T. The integration of the residual XAS profile with respect to the increase in energy is shown on the right vertical axis. For reference, the analysis after subtracting the oxide component (closed circles) is compared to that prior to the calibration (open circles).

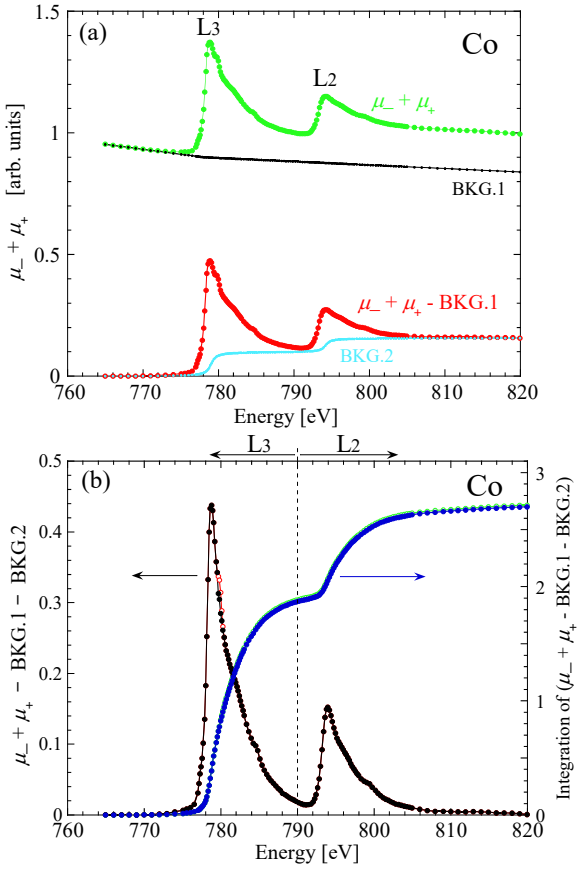

FIG. 7: (Color online) (a) XAS profiles $\mu_- + \mu_+$ for Co at H = 1.2 T. The residual XAS profile obtained after subtracting the assumed background (BKG.1) is shown along with BKG.2, which is composed of two arctangent functions (intensity ratio of 1.7:1.0). (b) XAS profiles after subtracting two background components (BKG.1 and BKG.2), $\mu_- + \mu_+$ - BKG.1 - BKG.2, for Co at H = 1.2 T. The integration of the residual XAS profile with respect to the increase in energy is shown on the right vertical axis. For reference, the analysis after subtracting the oxide component (closed circles) is compared to that prior to the calibration (open circles).

IV. DISCUSSION

To verify the reliability of the aforementioned analyses, the L_3 and L_2 intensities of XAS, *i.e.*, $I(L_3)$ and $I(L_2)$, were analyzed. According to Goering's sum rule correction, the mixing factor X was estimated using the ratio of each intensity at both the L_2 and L_3 edges (r_{23} in the literature) [12]. The spin correction factor (SC) was obtained as $SC = 1/(1-2X)$. In less than half of the $3d$ elements such as V and Cr, X has a negative value and the value of SC is much larger than 1. However, for Fe-metal, Co-metal, and Co-Heusler compounds, the X values were positive and estimated as -0.13, -0.17, and -0.17, respectively [12]. Consequently, the values of SC were 0.80, 0.74, and 0.74, respectively. In addition, X was significantly dependent on how the *arctan* step background was estimated for L_3 and L_2. In the present XMCD experiments, the calculation results were $r_{23} = 0.38$, X = -0.18, and $SC = 0.74$ for Fe and $r_{23} = 0.35$, X = -0.22, and $SC = 0.70$ for Co. Table III shows a comparison between the present results and the aforementioned results in the literature [12]. The present results are nearly consistent with those in the literature [12] in terms of both sign and magnitude. We can conclude that the present analyses have sufficient reliability in comparing the $m_{\rm orb}/m_{\rm spin}$ ratio of Fe and Co.

As mentioned in Section II, the saturated magnetization was 1.84×10^{-1} $\mu_{\rm B}$ per $Fe_{0.75}Co_{0.25}$. According to the DFT calculation, the average electrons in the d-orbitals for the nonmagnetic semiconductor FeSi and diamagnetic semimetal FeCo are 6.5 and 7.7, respectively [23]. It is assumed that in the series of $Fe_{1-x}Co_xSi$, there would be no large deviations between $n_{\rm h}$ for Fe and Co. We calculated the average $m_{\rm spin}$ values for Fe and Co, as shown in Table II. If the absolute value of the aforementioned average $m_{\rm spin}$, 1.26×10^{-1} $\mu_{\rm B}/n_{\rm h}$, is consistent with the observed saturated magnetization, 1.84×10^{-1} $\mu_{\rm B}$, the value of $n_{\rm h}$ for both Fe and Co was estimated to be 1.46. This value for $Fe_{0.75}$ $Co_{0.25}Si$ is smaller than the values for the two mother compounds FeSi and CoSi, 3.5 and 2.3, respectively, which were obtained through the DFT calculation [23]. Here, for both Fe and Co, $m_{\rm orb}$ has the same sign as $m_{\rm spin}$, suggesting that both moments are parallel to each other. This analytical result reveals that the electronic states for Fe and Co belong to the category of having more than half spins in the $3d$ state.

Below, we discuss the importance of the estimations of $m_{\rm orb}/n_{\rm h}$, $m_{\rm spin}/n_{\rm h}$, and $m_{\rm orb}/m_{\rm spin}$ for $Fe_{0.75}Co_{0.25}Si$ in the series of intermetallic compounds $Fe_{1-x}Co_xSi$, when they are considered as distorted alloys. The two parent compounds on either side of the $(Fe_{1-x}Co_x)Si$ solid solution are a nonmagnetic semiconductor and nonmagnetic metal, respectively [5]. The Fe substitution into the Co site brings about one-hole doping into the d-orbital, and $(Fe_{1-x}Co_x)Si$ for $x > 0.05$ becomes metallic [10]. The NMR measurements reveal that Co atoms, which have one or more Fe atoms in their nearest neighbor metal sites, become magnetic, whereas nonmagnetic Co atoms have no Fe atoms at their nearest neighbor metal sites [5]. Further, another DFT calculation reveals that the magnetic moments are distributed among the Fe and Co atoms [24]. Their atoms in $(Fe_{1-x}Co_x)Si$ are neither completely segregated nor completely intermixed. Both magnetic moments depend on the number of nearest-neighbor Co atoms for the corresponding atoms ($NN_{\rm Co}$). The magnetic moment for Fe varies from 0.1 to 0.5 $\mu_{\rm B}$ for $NN_{\rm Co} \leq 4$, whereas that for Co varies from 0.15 to 0.35 for $NN_{\rm Co} \leq 2$. In the present experiment, if $n_{\rm h} = 1.46$ is commonly adopted for both Fe and Co, the absolute values of $m_{\rm spin}$ for Fe and Co are estimated to be 0.174 and 0.193, respectively. According to the DFT calculations in Ref. [24], in $Fe_{0.75}Co_{0.25}Si$, $NN_{\rm Co}$ for Fe is estimated to be approximately 1, and $NN_{\rm Co}$ for Co is estimated to be approximately zero. In Ref. [24], the state $NN_{\rm Co} = 0$ for Co at $x = 0.25$ has the lowest energy arrangement. As suggested by the NMR measurement [5], the present experiment suggests that the adjacent arrangement of Fe and Co is important for stabilizing the magnetic moments. Since the atomic weight of Fe is not significantly different from that of Co, it is difficult to determine the atomic sites of Fe and Co independently. Hence, the above discussion on atomic sites is meaningful.

In $(Fe_{1-x}Co_x)Si$, $T_{\rm c}$ is the maximum at approximately $x = 0.35\sim0.40$, as shown in Fig. 1(a) [11]. At approximately $x = 0.2$ with a maximum value in k, the structural chirality changes from right-handed to left-handed [19]. Neutron diffraction revealed that the helix wave vector reached a maximum at $x = 0.20$, and the DM interaction reached a maximum at approximately $x = 0.2$, as shown in Fig. 1(b) [6–9, 11]. The $x = 0.25$ composition is the best to investigate L for both Fe and Co. The ratio of $m_{\rm orb}$ to $m_{\rm spin}$ was independently estimated to be $m_{\rm orb}/m_{\rm spin} \sim 3$ % for Fe and 9 % for Co. The spin-orbit coupling of Co was expected to be larger than that of Fe.

For reference, the XMCD conducted at the K-edges renders an element-specific probe with a higher bulk sensitivity of magneticelectronic properties than L-edge XMCD [25]. Through the $4p$ orbital hybridized to the $3d$ orbital, it was revealed that a nonmagnetic semiconductor at $x = 0$ transforms into a half-metallic ferromagnet when $0.08 \leq x \leq 0.25$, which becomes a strong ferromagnet when $x \geq 0.03$. The $x = 1.0$ composition stabilizes the diamagnetic semimetal.

The magnetocrystalline anisotropy arises from the SOC alone; the DM interaction arises from a combined second-order perturbation of the SOC and exchange interaction. The DM is linear in SOC. Herein, for simplicity, we consider two spins system $\vec{S}_{\rm i}$ (i = 1, 2). When the following Hamiltonian is given,

$$\mathcal{H} = \lambda \vec{L}_1 \cdot \vec{S}_1 + \lambda \vec{L}_2 \cdot \vec{S}_2 - J \vec{S}_1 \cdot \vec{S}_2, \qquad (11)$$

where $\vec{L}_{\rm i}$ (i = 1, 2) is orbital angular momentum and λ is the SOC coefficient, then, the DM interaction is defined

TABLE I: Estimation of A, B, C, D, C-$2D$, and $A/(C\text{-}2D)$, appearing in Eqs. (8)-(10), for Fe and Co in $Fe_{0.75}Co_{0.25}Si$. Two types of analytical results, with and without the contribution of oxides, are compared. For Co, the effect of oxides appears only in B.

	A	B	C	D	C-$2D$	$A/(C\text{-}2D)$
Fe including oxides	-3.88 $\times$ 10^{-2}	1.13 $\times$ 10^{1}	-2.50 $\times$ 10^{-1}	2.11 $\times$ 10^{-1}	-6.72 $\times$ 10^{-1}	5.77 $\times$ 10^{-2}
Co including oxides	-2.42 $\times$ 10^{-2}	2.72	-7.54 $\times$ 10^{-2}	5.12 $\times$ 10^{-2}	-1.78 $\times$ 10^{-1}	1.36 $\times$ 10^{-1}
Fe	-3.25 $\times$ 10^{-2}	1.09 $\times$ 10^{1}	-2.39 $\times$ 10^{-1}	2.06 $\times$ 10^{-1}	-6.51 $\times$ 10^{-1}	4.99 $\times$ 10^{-2}
Co	-2.42 $\times$ 10^{-2}	2.70	-7.54 $\times$ 10^{-2}	5.12 $\times$ 10^{-2}	-1.78 $\times$ 10^{-1}	1.36 $\times$ 10^{-1}

TABLE II: Estimation of $m_{\rm orb}/n_{\rm h}$ $(= 2A/(\frac{3}{2}B))$, $m_{\rm spin}/n_{\rm h}$ $(= 3(C-2D)/(\frac{3}{2}B))$, and $m_{\rm orb}/m_{\rm spin}$ $(= 2A/\{3(C-2D)\})$ for Fe and Co in $Fe_{0.75}Co_{0.25}Si$.

		Fe	Co	Average for Fe and Co
including oxides	$m_{\rm orb}/n_{\rm h}$ [$\mu_{\rm B}$]	-4.58 $\times$ 10^{-3}	-1.19 $\times$ 10^{-2}	–
	$m_{\rm spin}/n_{\rm h}$ [$\mu_{\rm B}$]	-1.19 $\times$ 10^{-1}	-1.31 $\times$ 10^{-1}	-1.25 $\times$ 10^{-1}
	$m_{\rm orb}/m_{\rm spin}$	3.85 $\times$ 10^{-2}	9.07 $\times$ 10^{-2}	–
subtracting oxides	$m_{\rm orb}/n_{\rm h}$ [$\mu_{\rm B}$]	-3.98 $\times$ 10^{-3}	-1.20 $\times$ 10^{-2}	–
	$m_{\rm spin}/n_{\rm h}$ [$\mu_{\rm B}$]	-1.19 $\times$ 10^{-1}	-1.32 $\times$ 10^{-1}	-1.26 $\times$ 10^{-1}
	$m_{\rm orb}/m_{\rm spin}$	3.33 $\times$ 10^{-2}	9.07 $\times$ 10^{-2}	–

as,

$$\mathcal{H}_{\rm DM} = \vec{D} \cdot (\vec{S_1} \times \vec{S_2}), \tag{12}$$

where the DM vector $\vec{D}$ is represented as,

$$|\vec{D}| = 2i\lambda J\Big[\sum_{n_1} \frac{< g_1|L_1|n_1 >}{\epsilon_{n_1} - \epsilon_{g_1}} - \sum_{n_2} \frac{< g_2|L_2|n_2 >}{\epsilon_{n_2} - \epsilon_{g_2}}\Big], \tag{13}$$

where $\epsilon_{g_{\rm i}}$ and $\epsilon_{n_{\rm i}}$ denote the energy level for ground state and excited states for $\vec{S_{\rm i}}$ (i = 1, 2), respectively [2]. Therefore, to numerically evaluate the DM interaction between $\vec{S_1}$ and $\vec{S_2}$, a heavy calculation is required to find the magnetic interaction between the two ground states via their excited states (n_1 and n_2). The findings of the study has the potential to be of use and interest for the theoreticians. In this study, an electron yield XMCD, which reflects magnetic information around the surface, was used. If sufficient efficiency of the electron yield can be obtained, the electron yield method can be applied to interfacial DM systems as well as the so-called bulk DM system.

TABLE III: Estimation of $I(L_3)$, $I(L_2)$, $I(L_2)/I(L_3)$ (= r_{23}), $I(L_3)$-$I(L_2)$, $2I(L_2)$-$I(L_3)$, $I(L_3)$+$I(L_2)$, X, and SC for Fe and Co in $Fe_{0.75}Co_{0.25}Si$. Here, $I(L_3)$ and $I(L_2)$ are the intensities of the XAS spectra, (μ_- + μ_+ - BKG.1 - BKG.2)/2, for L_3 and L_2 edges, respectively. In addition, $SC = 1/(1-2X)$, and $X = \{2I(L_2)$ - $I(L_3)\}/\{I(L_3) + I(L_2)\}$.

	$I(L_3)$	$I(L_2)$	$I(L_2)/I(L_3)$	$I(L_3)$-$I(L_2)$	$2I(L_2)$-$I(L_3)$	$I(L_3)$+$I(L_2)$	X	SC	Ref.
Fe	0.805	0.302	0.376	0.503	-0.200	1.11	-0.18	0.74	present study
Co	0.216	0.0761	0.352	0.140	-0.0638	0.291	-0.22	0.70	present study
Fe	-	-	0.41	-	-	-	-0.13	0.80	[12]
Co	-	-	0.38	-	-	-	-0.17	0.74	[12]
Co-Heusler	-	-	0.38	-	-	-	-0.17	0.74	[12]

V. CONCLUSION

We evaluated the ratio of the orbital magnetic moment $m_{\rm orb}$ to the spin magnetic moments $m_{\rm spin}$ for Fe and Co in $Fe_{0.75}Co_{0.25}Si$ with the maximum helix wave vector and maximum DM interaction. The ratio of $m_{\rm orb}$ to $m_{\rm spin}$ was independently estimated to be $m_{\rm orb}/m_{\rm spin} \sim 3$ % for Fe and 9 % for Co. The spin-orbit coupling of Co was expected to be larger than that of Fe. In both Fe and Co, the orbital magnetic moment was parallel to the spin counterpart. The hole number $n_{\rm h}$ in the d bands for Fe and Co was estimated to be approximately 1.5 when the averaged $m_{\rm spin}/n_{\rm h}$ for Fe and Co is compared with the saturated magnetization using a commercial SQUID magnetometer.

Utilizing previous DFT calculations, the numbers of nearest neighboring Co atoms for the Fe and Co atoms are estimated to be approximately 1 and zero, respectively. The DFT calculation suggests that the state $NN_{\rm Co} = 0$ for Co at $x = 0.25$ has the lowest energy arrangement, which is consistent with the actual analytical result. Finally, it was verified that the adjacent arrangement of Fe and Co is important for stabilizing the ferromagnetic state.

The $Fe_{0.75}Co_{0.25}Si$ crystal evaluated in this study has the left-handed chirality, whereas by reducing the value of x below 0.20, we can obtain the right-hand chirality. In the future, we will compare the sign of $m_{\rm orb}$ obtained for the left-handed and right-handed systems. Furthermore, we also intend to determine the $m_{\rm orb}$ for a representative B20-type helimagnet MnSi.

Acknowledgments

This XMCD experiment was conducted at KEK under the approval of KEK-PF, proposal No. 2020R-06. This study was supported by Grants-in-Aid for Scientific Research, Grant No. (S) 25220803, from the Ministry of Education, Culture, Sports, Science and Technology (MEXT), Japan. This study was also supported by the Center for Chiral Science at Hiroshima University (the MEXT program for promoting the enhancement of research universities, Japan) and the JSPS Core-to-Core Program, A. Advanced Research Networks.

Author Declarations

Conflict of Interest

The author has no conflicts to disclose.

Data Availability

The data that support the findings of this study are available from the corresponding author upon reasonable request.

[1] I. E. Dzyaloshinskii, J. Phys. Chem. Solids **4**, 241 (1958).
[2] T. Moriya, Phys. Rev. **120**, 91 (1960).
[3] M. Mito, H. Ohsumi, T. Shishidou, F. Kuroda, M. Weinert, K. Tsuruta, Y. Kotani, T. Nakamura, Y. Togawa, J. Kishine, et al., Phys. Rev. B **99**, 174439 (2019).
[4] W. Münzer, A. Neubauer, T. Adams, S. Mhlbauer, C. Franz, F. Jonietz, R. Georgii, P. Böni, B. Pedersen, M. Schmidt, et al., Phys. Rev. B **81**, 041203(R) (2010).
[5] S. Kawarazaki, H. Yasuoka, Y. Nakamura, and J. H. Wernick, J. Phys. Soc. Jpn. **41**, 1171 (1976).
[6] J. Beille, J. Voiron, F. Towfiq, M. Roth, and Z. Y. Zhang, J. Phys. F: Met. Phys. **11**, 2153 (1981).
[7] J. Beille, J. Voiron, and M. Roth, Solid State Commun. **47**, 399 (1983).
[8] K. Ishimoto, H. Yamauchi, Y. Yamaguchi, J. Suzuki, M. Arai, M. Furusaka, and Y. Endoh, J. Magn. Magn. Mater. **90** (1990).
[9] K. Ishimoto, Y. Yamaguchi, J. Suzuki, M. Arai, M. Furusaka, and Y. Endoh, Physica B **213** (1995).
[10] T. Susaki, T. Mizokawa, A. Fujimori, A. Ohno, T. Tonogai, and H. Takagi, Phys. Rev. B **58**, 1197 (1998).
[11] S. V. Grigoriev, S. V. Maleyev, V. A. Dyadkin, D. Menzel, J. Schoenes, and H. Eckerlebe, Phys. Rev. B **76**, 092407 (2007).
[12] E. Goering, Phil. Mag. **85**, 2895 (2005).
[13] B. T. Thole, P. Carra, F. Sette, and G. van der Laan, Phys. Rev. Lett. **68**, 1943 (1992).
[14] M. Altarelli, Phys. Rev. B **47**, 597 (1993).
[15] T. Jo, J. Phys. Soc. Jpn. **62**, 1814 (1993).
[16] Y. Teramura, A. Tanaka, and T. Jo, J. Phys. Soc. Jpn. **65**, 1053 (1996).
[17] Y. Kousaka, S. Iwasaki, T. Sayo, H. Tanida, T. Matsumura, S. Araki, J. Akimitsu, and Y. Togawa, Jpn. J. Appl. Phys. **00**, 00 (2022).
[18] G. M. Sheldrick, Acta Cryst. A **64**, 112 (2008).
[19] S. Grigoriev, D. Chernyshov, V. A. Dyadkin, V. Dmitriev, S. Maleyev, E. Moskvin, D. Menzel, J. Schoenes, and H. Eckerlebe, Phys. Rev. Lett. **102**, 037204 (2009).
[20] L. J. Bannenberg, A. J. E. Lefering, K. Kakurai, Y. Onose, Y. Endoh, Y. Tokura, and C. Pappas, Phys. Rev. B **94**, 134433 (2016).
[21] L. J. Bannenberg, K. Kakurai, P. Falus, E. Lelivre-Berna, R. Dalgliesh, C. D. Dewhurst, F. Q. andY. Onose, Y. Endoh, Y. Tokura, and C. Pappas, Phys. Rev. B **95**, 144433 (2017).
[22] J. Stöhr and H. C. Siegmann, *Magnetism, From Fundamentals to Nanoscale Dynamics* (Springer, Berlin Heidelberg New York, 2006).
[23] P. Dutta and S. K. Pandey, J. Phys.: Condens. Matter **31**, 145602 (2019).
[24] J. Guevara, V. Vildosola, J. Milano, and A. M. Llois, Phys. Rev. B **69**, 184422 (2004).
[25] G. R. Hearne, G. Diguet, F. Baudelet, J.-P.Itië, and N. Manyala, J. Magn. Magn. Mater. **379**, 274 (2015).